Inorganic Chemistry

pubs.acs.org/IC Article

Halogenated Gallium Corroles:DNA Interaction and Photodynamic Antitumor Activity

Ling-Gui Liu, Yan-Mei Sun, Ze-Yu Liu, Yu-Hui Liao,* Lei Zeng, Yong Ye, and Hai-Yang Liu*

Cite This: *Inorg. Chem.* 2021, 60, 2234−2245 Read Online

ACCESS | Metrics & More | Article Recommendations | Supporting Information

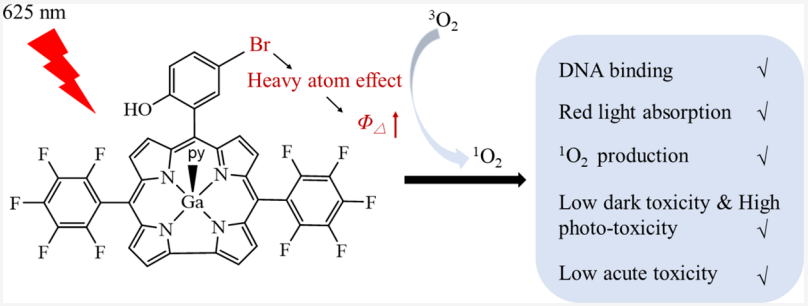

ABSTRACT: A series of halogenated gallium corroles were synthesized and characterized by UV−vis, HRMS, NMR, and FT-IR. The interaction between these gallium corroles and calf thymus DNA had been investigated by spectroscopic methods. These gallium corroles would interact with CT-DNA via an outside binding mode. The photodynamic antitumor activity in vitro of these gallium corroles toward different cell lines had also been tested. **3-Ga** displayed low cytotoxicity to normal cells under both light and dark conditions but high phototoxicity to liver cancer cells HepG2. The vitro experiment results showed that **3-Ga** could be efficiently absorbed by tumor cells. After light illumination, it may induce reactive oxygen species (ROS) and cause destruction of the mitochondrial membrane potential, which may finally trigger tumor cell apoptosis. Flow cytometry results showed that HepG2 cells were mainly distributed in the sub-G0 phase, which corresponds to cells with highly fragmented DNA or dead cells generally. This suggests that **3-Ga** could lead to tumor cell apoptosis after light illumination.

INTRODUCTION

Photodynamic therapy (PDT) has been developed as an emerging cancer treatment method. As compared to traditional cancer treatment methods such as chemotherapy, radiotherapy, and surgery, PDT has the advantages of little invasivity, low toxicity to normal tissues, less drug resistance, and controllable treatment area selection.[1] Porphyrin and its derivatives have been proved extensive applications in medicine.[2] Some porphyrin derivatives have been used as photosensitizers clinically in the photodynamic treatment of cancer.[3] Corrole is a tetrapyrrole macrocyclic compound similar to porphyrin. It has a smaller inner ring cavity, which enables corrole to coordinate with higher oxidation metal ions.[4] Because of their unique structure and electronic properties, corrole and metal corrole have been widely used in various fields, such as antitumor,[5] sensors,[6] and catalysis.[7]

Cancer has always been an intractable problem in the medical field, and the development of new and efficient anticancer drugs is an urgent task to be solved. Many anticancer drugs, such as chemotherapy drug cisplatinum, can crosslink with the purine bases on the DNA, interfering with DNA repair mechanisms, causing DNA damage, and subsequently inducing apoptosis in cancer cells.[8] Therefore, molecules with strong affinity for DNA are potential anticancer agents. Previous studies have shown that metal corroles had the ability to interact with DNA.[9] Here, we also have investigated the interaction between CT-DNA and halogenated gallium corroles in order to check their DNA binding affinity. It should be pointed out that the DNA binding between these gallium corroles and DNA in the nucleus is not expected when they are used as PDT photosensitizers, considering the risk of mutagenicity.

It is known that the heavy atom effect can improve the capability of the photosensitizer in producing singlet oxygen and enhance the PDT efficiency.[10] We found that halogen substituent at the meso-phenyl group of corroles may tune their photophysical properties via heavy-atom effects.[11] Heavier halogen atoms are able to reduce the fluorescence quantum yield and lifetime, leading to the increase of the intersystem crossing rate and improvement of singlet oxygen

Received: October 11, 2020
Published: January 22, 2021

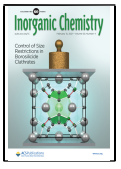

https://dx.doi.org/10.1021/acs.inorgchem.0c03016
Inorg. Chem. 2021, 60, 2234−2245

Scheme 1. Synthetic Procedure of the Halogenated Gallium(III) Corroles

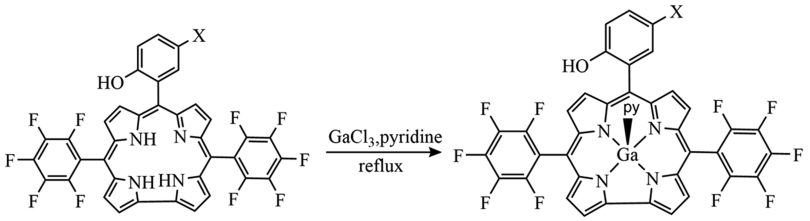

X= F (**1**), Cl (**2**), Br(**3**), I(**4**). X= F (**1-Ga**), Cl (**2-Ga**), Br (**3-Ga**), I (**4-Ga**).

quantum yield.[12] The center metal ions also have significant impacts on anti-tumor effects.[13] Gallium corrole complexes have been reported to exhibit good anti-tumor activities.[14] Early studies showed that gallium anionic corrole could penetrate the cell membrane and achieve tumor target delivery after binding the carrier protein.[15] Our previous work showed that the neutral gallium corrole could easily penetrate the cell membrane and produce singlet oxygen in the cell after illumination, resulting in cell apoptosis.[14] As compared with other metals such as iron, manganese, or copper, the introduction of gallium was found to be more efficient in enhancing the PDT activity of freebase corrole.[16] Hence, in order to facilitate PDT activity of corrole derivatives by using the heavy atom effect and gallium, we hereby wish to report the preparation of a series of halogenated gallium corroles (Scheme 1) and their photodynamic antitumor activity toward tumor cells in vitro. Their DNA binding capability and acute toxicity were also tested. It turned out that **3-Ga** generated singlet oxygen as effective reactive oxygen species with a high quantum yield due to the heavy atom effect and exhibited remarkable PDT activity under near-IR light with selectivity toward liver cancer cells (HepG2) over normal cells.

EXPERIMENTAL SECTION

Materials. All reagents were purchased commercially and not further purified prior to using unless specifically mentioned. The ultrapure water was used in all biological experiments. ^{1}H, ^{19}F, and ^{13}C nuclear magnetic resonance (NMR) spectra were recorded on a Bruker Ascend 500 spectrometer in $CDCl_3$ or DMSO-d_6 solution. High-resolution mass spectrometry (HRMS) spectra were acquired by a Bruker maXis impact mass spectrometer with an electrospray ionization source. The UV−vis absorption spectra were obtained using a Hitachi 3900H UV−vis spectrometer, and the fluorescence emission spectra were measured with a Hitachi F-4500 fluorescence spectrophotometer at room temperature. The Fourier transform infrared (FT-IR) spectrum was obtained on a Bruker Vertex 70 FT-IR spectrometer. The electron paramagnetic resonance (EPR) spectrum was detected by a Bruker Elexsys-II E500 CW-EPR spectrometer. The cells were observed by using an Olympus IX73 fluorescence microscope, Nikon Ti2-U fluorescence microscope, and Leica TCS SP8 laser scanning confocal microscope. A BD FACS Celesta flow cytometer was used for flow cytometry analysis. The light source for photodynamic therapy was from a red LED lamp (625 ± 2 nm, 3 W/m^2). All cell lines were bought from the American Type Culture Collection, and the BALB/c mice were purchased from the laboratory animal center of South China University of Technology.

Synthesis of Free Base Corroles. 10-(2-Hydroxyl-5-fluorophenyl)-5,15-bis(pentafluorophenyl)corrole (**1**), 10-(2-hydroxyl-5-chlorophenyl)-5,15-bis(pentafluorophenyl)corrole (**2**), 10-(2-hydroxyl-5-bromophenyl)-5,15-bis(pentafluorophenyl)corrole (**3**), and 10-(2-hydroxyl-5-iodophenyl)-5,15-bis(pentafluorophenyl)corrole (**4**) were synthesized according to the procedures described in the Supporting Information.

*10-(2-Hydroxyl-5-fluorophenyl)-5,15-bis(pentafluorophenyl)-corrole (**1**).* UV−vis (CH_2Cl_2), λ_{max}/nm (logε/(M^{-1} cm^{-1})): 412 (5.18), 565 (4.40), 613 (4.18). ^{1}H NMR (400 MHz, $CDCl_3$) δ 9.11 (d, J = 4.2 Hz, 2H), 8.75 (d, J = 4.5 Hz, 2H), 8.68 (d, J = 4.7 Hz, 2H), 8.58 (d, J = 4.1 Hz, 2H), 7.65 (dd, J = 8.4, 2.8 Hz, 1H), 7.40 (td, J = 8.6, 2.8 Hz, 1H), 7.25−7.21 (m, 1H). ^{19}F NMR (471 MHz, $CDCl_3$) δ −125.05 (s), −137.83 (dd, J = 25.2, 6.6 Hz), −152.34 (t, J = 20.8 Hz), −161.50 (ddd, J = 30.1, 22.6, 8.5 Hz). HRMS-ESI: m/z: calcd for $C_{37}H_{16}F_{11}N_4O$: 741.1143, found: 741.1151 [M + H$^+$].

*10-(2-Hydroxyl-5-chlorophenyl)-5,15-bis(pentafluorophenyl)-corrole (**2**).* UV−vis (CH_2Cl_2), λ_{max}/nm (logε/(M^{-1} cm^{-1})): 412 (5.09), 565 (4.33), 613 (4.13). ^{1}H NMR (500 MHz, $CDCl_3$) δ 9.11 (d, J = 4.2 Hz, 2H), 8.74 (d, J = 4.6 Hz, 2H), 8.67 (d, J = 4.6 Hz, 2H), 8.58 (d, J = 4.1 Hz, 2H), 7.91 (d, J = 2.1 Hz, 1H), 7.64 (dd, J = 8.8, 2.1 Hz, 1H), 7.23 (d, J = 8.8 Hz, 1H). ^{19}F NMR (471 MHz, $CDCl_3$) δ −137.84 (dd, J = 25.5, 8.6 Hz), −152.30 (t, J = 21.8 Hz), −161.49 (dd, J = 31.2, 7.6 Hz). HRMS-ESI: m/z: calcd for $C_{37}H_{16}ClF_{10}N_4O$: 757.0847, found: 757.0863 [M + H$^+$].

*10-(2-Hydroxyl-5-bromophenyl)-5,15-bis(pentafluorophenyl)-corrole (**3**).* UV−vis (CH_2Cl_2), λ_{max}/nm (logε/(M^{-1} cm^{-1})): 412 (5.13), 565 (4.34), 613 (4.11). ^{1}H NMR (500 MHz, $CDCl_3$) δ 9.11 (d, J = 4.2 Hz, 2H), 8.75 (d, J = 4.6 Hz, 2H), 8.67 (d, J = 4.7 Hz, 2H), 8.59 (d, J = 4.2 Hz, 2H), 8.05 (d, J = 2.4 Hz, 1H), 7.78 (dd, J = 8.8, 2.4 Hz, 1H), 7.17 (d, J = 8.8 Hz, 1H). ^{19}F NMR (471 MHz, $CDCl_3$) δ −137.83 (dd, J = 25.8, 10.1 Hz), −152.26 (t, J = 21.9 Hz), −161.45 (dd, J = 29.4, 6.3 Hz). HRMS-ESI: m/z: calcd for $C_{37}H_{16}BrF_{10}N_4O$: 801.0342, found: 801.0356 [M + H$^+$].

*10-(2-Hydroxyl-5-iodophenyl)-5,15-bis(pentafluorophenyl)-corrole (**4**).* UV−vis (CH_2Cl_2), λ_{max}/nm (logε/(M^{-1} cm^{-1})): 412 (5.05), 565 (4.25), 613 (4.00). ^{1}H NMR (500 MHz, $CDCl_3$) δ 9.12 (d, J = 4.2 Hz, 2H), 8.75 (d, J = 4.6 Hz, 2H), 8.67 (d, J = 4.6 Hz, 2H), 8.59 (d, J = 4.1 Hz, 2H), 8.24 (s, 1H), 7.96 (d, J = 8.7 Hz, 1H), 7.08 (d, J = 8.7 Hz, 1H). ^{19}F NMR (471 MHz, $CDCl_3$) δ −137.83 (dd, J = 25.6, 9.4 Hz), −152.25 (t, J = 21.8 Hz), −160.31 − −162.83 (m). HRMS-ESI: m/z: calcd for $C_{37}H_{16}F_{10}IN_4O$: 849.0204, found: 849.0218 [M + H$^+$].

Synthesis of Gallium(III) Corroles. *10-(2-Hydroxyl-5-fluorophenyl)-5,15-bis(pentafluorop-henyl)corrole gallium (III) (**1-Ga**).* A total of 30 mg corrole **1** (0.037 mmol) was dissolved in 10 mL pyridine, and 70 mg $GaCl_3$ (0.4 mmol) was added. The mixture was stirred for 2 h under a nitrogen atmosphere at 120 °C. The reaction mixture was cooled down to room temperature. Then, 30 mL CH_2Cl_2 was added to the reaction mixture. The resulted solution was washed with saturated brine five times, and the organic layer was collected and dried by using anhydrous sodium sulfate. CH_2Cl_2 solvent was removed by a rotary evaporator, and the crude product was obtained. The product was purified by silica gel column chromatography using CH_2Cl_2/CH_3OH (100:1) as eluent. A purple-red solid product was obtained by recrystallization with CH_2Cl_2/hexane as the solvent. Yield: 82.3%. ^{1}H NMR (500 MHz, DMSO-d_6) δ 9.39 (s, 1H), 9.29 (s, 2H), 8.98 (s, 2H), 8.89 (s, 2H), 8.68 (s, 2H), 8.46 (s, 2H), 7.79−7.69 (m, 2H), 7.47 (t, J = 8.5 Hz, 1H), 7.38−7.32 (m, 2H), 7.31−7.24 (m, 1H). ^{19}F NMR (471 MHz, DMSO-d_6) δ −127.22 (s), −139.08 (d, J = 30.5 Hz), −154.66 − −156.08 (m), −162.43 − −164.19 (m). ^{13}C NMR (126 MHz, DMSO-d_6) δ 156.01, 154.15, 149.83, 147.17, 145.34, 143.95, 140.94, 136.81, 134.79, 130.11, 129.83, 127.22, 126.13, 124.65, 121.72, 121.55, 118.00, 116.45, 116.06, 107.08, 96.67. HRMS-ESI: m/z: calcd for $C_{37}H_{12}F_{11}GaN_4NaO$: 828.9983, found: 828.9986 [M-pyridine + Na] $^+$.

https://dx.doi.org/10.1021/acs.inorgchem.0c03016
Inorg. Chem. 2021, 60, 2234−2245

*10-(2-Hydroxyl-5-chlorophenyl)-5,15-bis(pentafluorophenyl)-corrole gallium (III) (**2-Ga**).* The synthetic procedures were similar to **1-Ga**. Yield: 81.6%. ^{1}H NMR (500 MHz, DMSO-d^6) δ 9.70 (s, 1H), 9.29 (s, 2H), 8.99 (s, 2H), 8.90 (s, 2H), 8.66 (s, 2H), 8.47 (s, 2H), 7.93 (s, 1H), 7.79−7.62 (m, 2H), 7.39−7.28 (m, 3H). ^{19}F NMR (471 MHz, $CDCl_3$) δ −135.54 − −137.24 (m), −153.65 (s), −160.75 − −162.52 (m). ^{13}C NMR (126 MHz, DMSO-d_6) δ 158.99, 156.73, 149.87, 147.22, 145.31, 143.94, 140.95, 136.80, 134.78, 130.63, 129.48, 127.24, 126.05, 124.95, 124.37, 122.07, 118.02, 117.36, 116.00, 106.77, 96.72. HRMS-ESI: *m/z*: calcd for $C_{37}H_{12}ClF_{10}GaN_4NaO$: 844.9688, found: 844.9711 [M-pyridine + Na] $^+$.

*10-(2-Hydroxyl-5-bromophenyl)-5,15-bis(pentafluorophenyl)-corrole gallium (III) (**3-Ga**).* The synthetic procedures were similar to **1-Ga**. Yield: 80.7%. ^{1}H NMR (500 MHz, DMSO-d_6) δ 9.77 (d, J = 11.4 Hz, 1H), 9.29 (d, J = 3.1 Hz, 2H), 9.00 (s, 2H), 8.90 (s, 2H), 8.67 (s, 2H), 8.41 (dd, J = 24.5, 6.7 Hz, 2H), 8.06 (s, 1H), 7.84−7.66 (m, 2H), 7.39−7.24 (m, 3H). ^{19}F NMR (471 MHz, DMSO-d_6) δ −139.07 (d, J = 32.4 Hz), −155.32 (d, J = 23.0 Hz), −163.22 (d, J = 27.2 Hz). ^{13}C NMR (126 MHz, DMSO-d_6) δ 157.17, 149.89, 145.28, 143.94, 140.94, 138.85, 137.52, 136.78, 136.61−136.58, 134.83, 132.39, 131.20, 127.28, 126.06, 124.97, 124.36, 117.98, 115.99, 109.69, 106.73, 96.75. HRMS-ESI: *m/z*: calcd for $C_{37}H_{12}BrF_{10}GaN_4NaO$: 888.9183, found: 888.9243 [M-pyridine + Na] $^+$.

*10-(2-Hydroxyl-5-iodophenyl)-5,15-bis(pentafluorophenyl)-corrole gallium (III) (**4-Ga**).* The synthetic procedures were similar to **1-Ga**. Yield: 85.4%. ^{1}H NMR (500 MHz, DMSO-d_6) δ 9.72 (s, 1H), 9.29 (s, 2H), 8.97 (s, 2H), 8.89 (s, 2H), 8.64 (s, 2H), 8.50 (s, 2H), 8.19 (s, 1H), 7.92 (d, J = 7.3 Hz, 1H), 7.77 (s, 1H), 7.37 (s, 2H), 7.15 (d, J = 8.1 Hz, 1H). ^{19}F NMR (471 MHz, DMSO-d_6) δ −139.08 (d, J = 29.3 Hz), −154.64 − −156.09 (m), −163.25 (d, J = 24.3 Hz). ^{13}C NMR (126 MHz, DMSO-d_6) δ 157.73, 149.84, 147.16, 145.28, 143.93, 143.35, 140.93, 140.34, 138.84, 138.20, 136.84, 134.80, 131.70, 127.22, 126.08, 124.92, 124.42, 118.25, 106.77, 96.69, 80.61. HRMS-ESI: *m/z*: calcd for $C_{37}H_{12}F_{10}GaIN_4NaO$: 936.9044, found: 936.9053 [M-pyridine + Na] $^+$.

UV−vis Absorption Spectrum Titration Experiment. The gallium corroles were diluted to 3 mM with DMF. Buffer solution I (5 mM Tris, 50 mM NaCl, HCl, pH = 7.2) was mixed with DMF as the control solution. Then, the gallium corrole solution (5 μL, 3 mM) was mixed with the control solution as the sample solution, keeping the concentration of gallium corrole constant. The UV−vis absorption spectrum of the sample solution was recorded ranging from 300 to 800 nm. After that, CT-DNA (2 μL, 1.5 mM) was added into the control solution and the sample solution successively, and the absorption spectrum was recorded after waiting for 5 min at a time. The measurement was stopped when the change in the spectrum was small. The intrinsic binding constant (K_b) of the samples with CT-DNA can be obtained by following equation:[17]

$$\frac{[DNA]}{\varepsilon_a - \varepsilon_f} = \frac{[DNA]}{\varepsilon_b - \varepsilon_f} + \frac{1}{K_b(\varepsilon_b - \varepsilon_f)} \quad (1)$$

where ε_a is the extinction coefficient of the compound in the presence of DNA, ε_f and ε_b are the extinction coefficient of the compound when bound to DNA incompletely and completely respectively, [DNA] is the concentration of DNA. K_b is the ratio of the slope to the intercept of the graph of $[DNA]/(\varepsilon_a - \varepsilon_f)$ versus [DNA].

Fluorescence Spectrum Titration Experiment. First, gallium corrole (5 μL, 3 mM) was mixed with solution of buffer I and DMF as the sample solution, keeping the concentration of gallium corrole constant. The fluorescence emission spectrum of the sample solution was recorded with appropriate excitation wavelength. After that, CT-DNA (2 μL, 1.5 mM) was added into the sample solution successively, and fluorescence emission spectrum was recorded after waiting for 5 min at a time. The measurement was stopped when the change in the spectrum was small. The quenching constants (K_{sv}) can be obtained by following Stern−Volmer equation:[18]

$$\frac{F_0}{F} = 1 + K_{sv}[Q] \quad (2)$$

where [Q] is the concentration of CT-DNA and F_0 and F are the fluorescence intensities in the absence and presence of CT-DNA, respectively.

Singlet Oxygen Detection. The absorbance of 1,3-diphenylisobenzofuran (DPBF) would decrease as a result of reaction with singlet oxygen. Therefore, DPBF was used as a singlet oxygen capture agent to detect the singlet oxygen quantum yield of gallium corroles by measuring the change of its absorbance. The solution of DPBF (40 μM) in DMF was prepared in the absence (control) and presence of gallium corroles (10 μM), and then the absorption spectrum was determined every 10 s after light irradiation (625 ± 2 nm, 3 W/m^2) at room temperature. Meanwhile, 5,10,15,20-tetraphenylporphyrin (TPP) was used as a reference substance to evaluate the singlet oxygen production of gallium corroles. The values of Φ_Δ were calculated by the following equation:[19]

$$\Phi_\Delta = \Phi_{Ref} \times \frac{K_{Sample}}{K_{Ref}} \times \frac{F_{Ref}}{F_{Sample}} \quad (3)$$

where k is the slope of the plot of DPBF absorbance (at 417 nm) *vis* irradiation time and F is the absorption correction factor given by $F = 1-10^{-OD}$ (OD is optical density of photosensitizer at the irradiation wavelength).

The ability to generate singlet oxygen of gallium corroles was further confirmed by using the electron paramagnetic resonance (EPR). TEMP and DABCO were used as a trapping agent and a quenching agent for singlet oxygen, respectively.

Photostability Study. The photostability of gallium corroles was studied by UV−vis absorption spectroscopy. The absorption spectra of gallium corroles solution (10 μM, in DMF/Tris) under different illumination times were determined. Each exposure time was 10 min (625 ± 2 nm, 3 W/m^2).

Aggregation Study in Solution. The possible aggregation of gallium corroles was investigated by UV−vis absorption spectroscopy. The absorption spectra of gallium corroles solution in different concentrations were determined. The change of the Soret band was monitored to determine whether the gallium corroles had self-aggregation in solution.

Cytotoxicity Assays. Inhibition of cell growth by gallium corroles was measured by a 3-(4,5-dimethylthiazole)-2,5-diphenyltetraazolium bromide (MTT) assay. First, cells were seeded in 96-well plates at a density of 5 × 10^3 cells per well and cultured in a cell incubator (37 °C, 5% CO_2) overnight. A series of gallium corroles were dissolved with DMSO (final concentration ≤ 1% *V*/*V* in the culture medium) and diluted by a DMEM medium to obtain different concentrations of samples. Then, samples of different concentrations were added into cell plates and cells of control wells were treated with the same conditions without gallium corroles. After culturing for 4 h, the cells were illuminated by red light (625 ± 2 nm, 3 W/m^2) for 1 h, and subsequently, the cells were incubated for another 24 h. After that, the culture medium with samples was removed and the culture medium with MTT dye solution (20 μL, 5 mg/mL) was added into all wells. After 4 h, DMSO (100 μL) was used to replace the culture medium. The optical density (OD) value of cell plates was acquired by a Thermo Scientific Microplate Reader at 495 nm. In order to minimize the error, each experiment was repeated three times.

Cellular Uptake. HepG2 cells were first cultured in glass-bottomed dishes (20 mm) with approximately 2 × 10^5 cells in each well for 24 h in a 5% CO_2 incubator at 37 °C. Then, the cells were treated with **3-Ga** (10 μM) and incubated for 4 h. After that, the cells were stained with 2-(4-amidinophenyl)-6-indolecarbamidine (DAPI) and washed with PBS solution for three times. Finally, the cells were observed and photographed with laser confocal fluorescence microscopy (oil objective 63×; magnification 630×; laser intensity 15%; gain at 800 V; DAPI excitation laser, 405 nm; DAPI detector, 410−500 nm; **3-Ga** excitation laser, 561 nm; **3-Ga** detector, 570−720 nm).

https://dx.doi.org/10.1021/acs.inorgchem.0c03016
Inorg. Chem. 2021, 60, 2234−2245

Flow cytometry was used to further detect the time-dependent uptake. HepG2 cells were first cultured in a 12-well plate for 24 h. After that, previous medium was replaced with a new medium containing **3-Ga** (10 μM). Fluorescence intensity was measured after additional incubation for 2, 4, and 6 h.

Reactive Oxygen Species (ROS) Detection in Cells. HepG2 cells were seeded in 12-well plates with approximately 2×10^5 cells in each well and incubated in a cell incubator for 24 h. Then, **3-Ga** (10 μM) were added into the wells. The cells were cultured for 4 h and exposed to light irradiation as previously described. After further incubation for 24 h, the culture medium was removed and the medium containing 2′,7′-dichlorodihydrofluorescein diacetate (DCFH-DA, 10 μM) was added. After sustained incubation for 30 min, the cells were rinsed with PBS for three times and observed under a fluorescence microscope (magnification 100×; exposure 200 ms; gain 3.4×; DCFH-DA excitation, 488 nm; DCFH-DA emission, 525 nm).

Mitochondrial Membrane Potential Assay. HepG2 cells were seeded in 12-well plates at a density of 2×10^5 cells per well and incubated in a cell incubator for 24 h. Afterward, the cells were treated with **3-Ga** (10 μM) and illuminated as previously described immediately after incubation for 4 h. Followed by incubation for 24 h, the medium containing 5,5′,6,6′-tetrachloro-1,1′,3,3′- tetraethylimidacarbocyanine iodide (JC-1) was injected into each well and incubated for another 20 min in a cell incubator. After that, the cells were washed with PBS over three times and observed with a fluorescence microscope (magnification 100×; exposure 800 ms; gain 17.1×; JC-1 monomers excitation, 490 nm; JC-1 monomers emission, 530 nm; JC-1 aggregates excitation, 525 nm; JC-1 aggregates emission, 590 nm).

Apoptosis Assay by Flow Cytometry. For the apoptosis assay, HepG2 cells were first seeded in 6-well plates for 24 h (37 °C in 5% CO_2). Then, the cells were incubated with the culture medium containing **3-Ga** (10 μM) or not. After further incubation for 4 h, the cells of light group were given irradiation (625 ± 2 nm, 3 W/m^2) for 1 h and sequentially cultured for 24 h. After that, the cells were collected, centrifuged, resuspended with PBS, re-centrifuged, and then stained with propidium iodide (PI, 50 mg/mL) and Annexin V-FITC (1 mg/mL) in PBS. At last, apoptosis was detected by using a BD FACS Celesta flow cytometer.

Cell Cycle Assay. For the cell cycle assay, HepG2 cells were cultured in 6-well plates. After incubating for 24 h (37 °C in 5% CO_2), the previous culture medium was replaced by a fresh culture medium containing **3-Ga** (10 μM) or not and irradiation was given to the cells of light group after 4 h. After 1 day, the cells were collected, centrifuged, resuspended with PBS, re-centrifuged, and then fixed with 70% ice ethanol at 4 °C overnight. After that, the cells were centrifuged, resuspended with PBS, re-centrifuged, and stained with RNase A (0.2 mg/mL) and PI (0.02 mg/mL) for 30 min at 37 °C in the dark. Finally, cell cycle was analyzed by using a BD FACS Celesta flow cytometer.

Acute Toxicity Studies In Vivo. Acute toxicity in vivo of **3-Ga** was tested by using BALB/C mice (4−5 weeks). The mice were divided into four groups (two groups of females and two groups of males) at random, and each group consists of three mice. The mice of experimental groups were injected **3-Ga** in a single dose of 10 mg/kg through the tail vein. The mice of control groups were given a single injection of 100 μL normal saline. After administration, the body weight, behavioral characteristics, and possible symptoms of the mice were monitored every day. Two weeks after the injection, the mice were euthanized, and their major organs, including the heart, liver, spleen, lung, and kidney, were quickly removed and weighed. Then, the organ coefficients were obtained by the ratio of the weight of each organ to the body weight of mice.

RESULTS AND DISCUSSION

Synthesis and Characterization. Corroles **1**−**4** were obtained according to a method published formerly and characterized by ^{1}H NMR, ^{19}F NMR spectroscopy, UV−vis spectroscopy, and mass spectrometry (HRMS-ESI). All gallium corroles were obtained by the reflux reaction of gallium chloride and freebase corroles in pyridine solvent under the protection of nitrogen. The final products were separated and

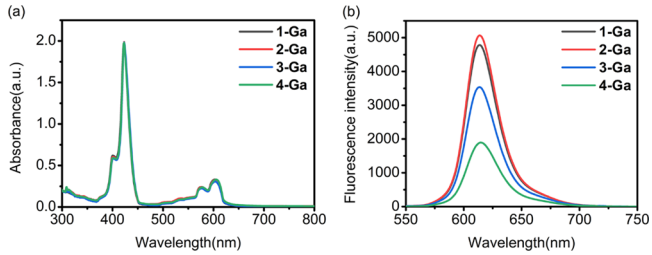

Figure 1. UV−visible absorption spectrum (a) and fluorescence emission spectrum (b) (λ_{ex} = 434 nm) of **1-Ga**, **2-Ga**, **3-Ga**, and **4-Ga** in DMF solution (10 μM).

Table 1. Photophysical Data of Gallium Corroles

	absorption [nm] (logε(M^{-1} cm^{-1}))					
corrole	Soret band	Q band		λ_{em} (nm)	Φ_F [a]	$\Phi_\triangle$ [b]
1-Ga	423(5.29)	576(4.38)	603(4.52)	613	0.33	0.18
2-Ga	423(5.30)	576(4.38)	604(4.52)	613	0.32	0.24
3-Ga	423(5.30)	576(4.35)	604(4.48)	613	0.22	0.32
4-Ga	423(5.35)	577(4.47)	605(4.61)	614	0.13	0.25

[a]TPP as a reference in toluene (Φ_F = 0.11).[21] [b]TPP as a reference in DMF ($\Phi_\triangle$ = 0.62).[22]

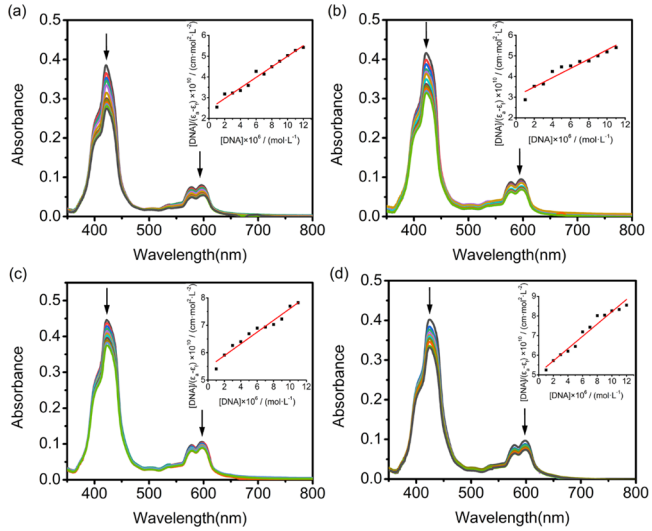

Figure 2. Changes in absorption spectra of **1-Ga** (a), **2-Ga** (b), **3-Ga** (c), and **4-Ga** (d) upon consecutive addition of CT-DNA.

Table 2. Intrinsic Binding Constants of Gallium Corroles Binding with CT-DNA

corrole	$\Delta\lambda$[a] (nm)	H[bb](%)	K_b (×10^5 L/mol)	K_{sv} (×10^4 L/mol)
1-Ga	1	28.62	1.04 ± 0.09	6.13 ± 0.64
2-Ga	1	24.35	0.73 ± 0.10	5.90 ± 0.45
3-Ga	1	15.91	0.39 ± 0.03	5.22 ± 0.61
4-Ga	0	17.47	0.62 ± 0.05	3.25 ± 0.38

[a]$\Delta\lambda$ represents the red shift of the Soret band induced by interaction between gallium corroles and CT-DNA. [b]H represents the hypochromism of Soret band obtained by $H\%$ = $(A_{free} - A_{bound})/A_{free} \times 100\%$.

https://dx.doi.org/10.1021/acs.inorgchem.0c03016
Inorg. Chem. 2021, 60, 2234−2245

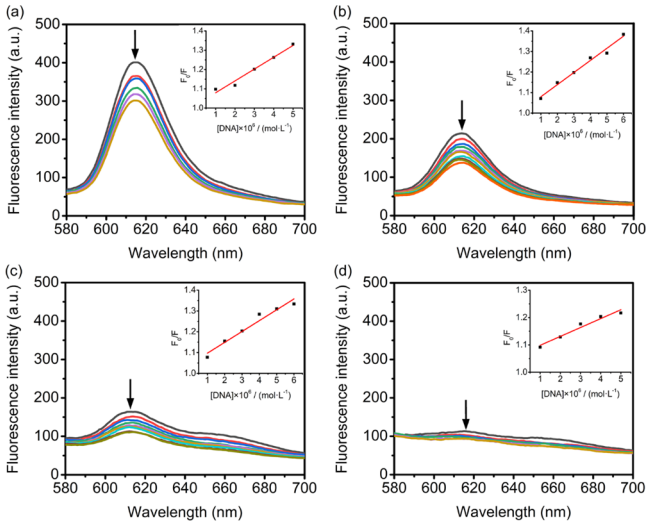

Figure 3. Changes in fluorescence spectra of **1-Ga** (a), **2-Ga** (b), **3-Ga** (c), and **4-Ga** (d) upon consecutive addition of CT-DNA.

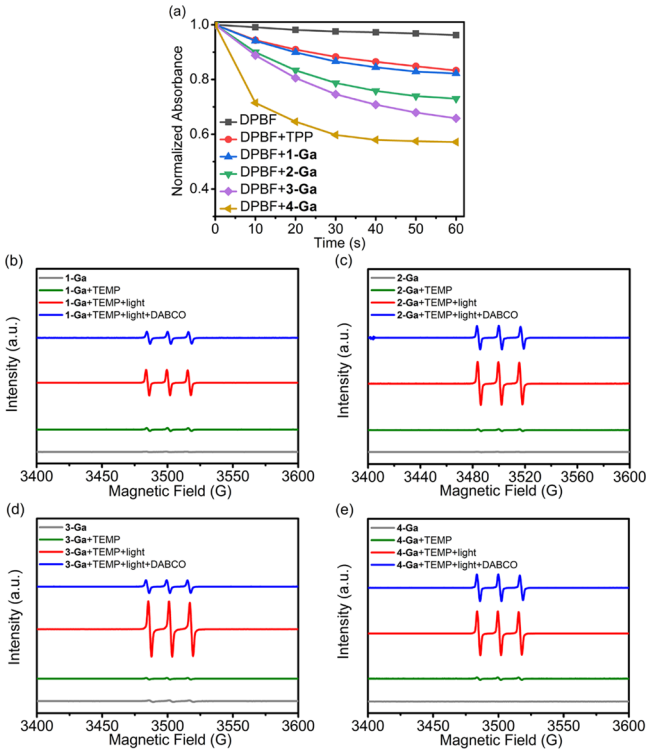

Figure 4. (a) Changes in absorbance of DPBF (417 nm) in the presence of gallium corroles (10 μM) with the irradiation time (625 ± 2 nm, 3 W/m^2). EPR spectra of **1-Ga** (b), **2-Ga** (c), **3-Ga** (d), and **4-Ga** (e) after irradiation in the presence of the trapping agent (TEMP) and quenching agent (DABCO).

purified by column chromatography and well characterized by ^{1}H NMR, ^{19}F NMR, ^{13}C NMR spectroscopy, UV−vis spectroscopy, HRMS-ESI, and FT-IR (Figures S1−S32).

Photophysical Properties. The photophysical properties of the gallium corroles were measured in DMF solutions. Figure 1a shows UV−vis spectrum of prepared gallium corroles, which exhibited similar typical absorption spectra characteristics. The gallium corroles exhibited an intense Soret band centered at 423 nm, arisen due to the $\pi-\pi^*$ electronic transition from the ground state (S0) to the second excited state (S2), and three weak Q bands at 500−650 nm, attributed to $\pi-\pi^*$ electronic transitions from the ground state (S0) to the first excited state (S1).[20] The type of halogen atom introduced seemed to have no obvious effect on the maximum absorption wavelength of gallium corroles. As shown in Figure 1b, all gallium corroles exhibited strong fluorescence with a maximum peak around 613 nm. The fluorescence intensity and fluorescence quantum yield (Φ_F) of gallium corroles decreased due to the heavy atom effect. All photophysical data of the gallium corroles are listed in Table 1.

Table 3. IC$_{50}$ (μM) Values of Gallium Corroles toward Various Tumor Cells

tumor cell		1-Ga	2-Ga	3-Ga	4-Ga	temoporfin
231						
	dark	>100	>100	>100	>100	47.4 ± 16.9
	light	1.3 ± 0.1	>100	>100	74.4 ± 18.9	0.6 ± 0.3
A549						
	dark	>100	>100	>100	>100	>100
	light	10.9 ± 2.5	47.2 ± 8.0	>100	>100	0.5 ± 0.2
HepG2						
	dark	>100	46.9 ± 20.6	>100	>100	71.5 ± 14.8
	light	9.3 ± 1.1	4.8 ± 13	10.0 ± 1.6	9.9 ± 2.0	8.4 ± 1.8
HSF						
	dark	>100	>100	>100	>100	>100
	light	1.3 ± 0.6	69.2 ± 19.9	94.5 ± 18.7	43.3 ± 5.3	1.5 ± 0.4
Huvec						
	dark	>100	>100	>100	>100	>100
	light	26.7 ± 3.7	>100	97.0 ± 17.5	>100	2.1 ± 0.2
[a]SI		0.1	14.4	9.4	4.4	0.2
[b]SI		2.9	>1.4	9.7	>10.1	0.25

[a]SI = light IC$_{50}$ values of HSF/light IC$_{50}$ values of HepG2. [b]SI = light IC$_{50}$ values of Huvec/light IC$_{50}$ values of HepG2.

Table 4. Chemical Properties of Prepared Gallium Corroles[d]

compounds	Mr[a]	tPSA[b]	cLogP[c]
1-Ga	806.00	35.85	13.52
2-Ga	821.97	35.85	14.09
3-Ga	865.92	35.85	14.24
4-Ga	913.91	35.85	14.50

[a]Molecular weight. [b]Calculation of the polar surface area based on fragment contributions. [c]Calculated logP based on the Biobyte algorithm. [d]ChemBioDraw Ultra (version 14.0).

DNA Binding. UV−vis absorption spectrum titration experiment is one of the simplest and most commonly used ways to identify binding mode between compound and DNA. When the complex binds to DNA, the surrounding environment of the complex changes, and the electronic structure is disturbed, resulting in the change of UV−vis absorption spectrum of the complex. The binding strength and binding pattern between the complex and DNA can be inferred from the spectral variation. As for porphyrins, the intercalative binding commonly generates an obvious red shift ($\Delta\lambda \geq 15$ nm) and a large hypochromism ($H \geq 35\%$), and the outside binding mode usually induces a slight red shift ($\Delta\lambda \leq 8$ nm) and a small hypochromism ($H \leq 10\%$).[23] Figure 2 displays

https://dx.doi.org/10.1021/acs.inorgchem.0c03016
Inorg. Chem. 2021, 60, 2234−2245

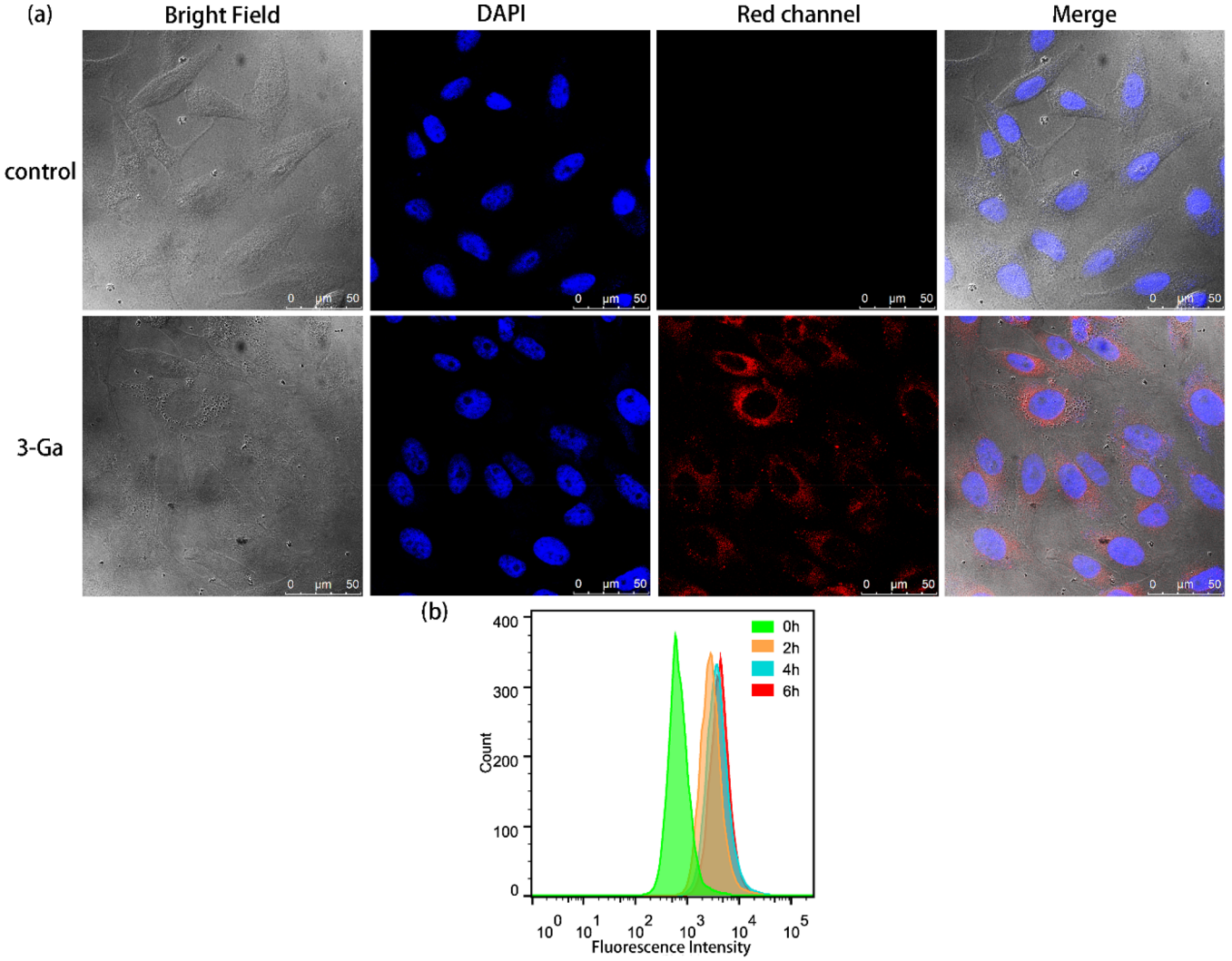

Figure 5. (a) Confocal images of HepG2 treated with **3-Ga** (10 μM) and stained with DAPI (scale bar is 50 μm). (b) Time-dependent uptake of **3-Ga** (10 μM) in HepG2 cells detected by flow cytometry.

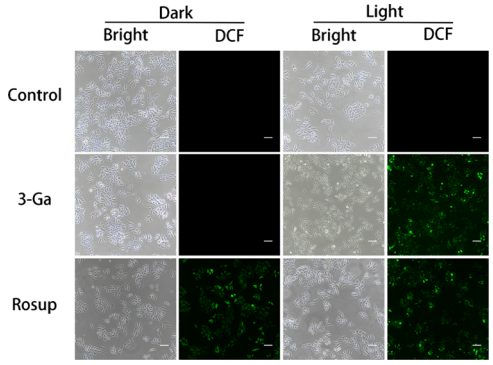

Figure 6. Intracellular ROS generation induced by **3-Ga** (10 μM) in HepG2 cells upon irradiation (625 ± 2 nm, 3 W/m^2, 1 h) using DCFH-DA as a probe (scale bar is 100 μm).

electronic absorption spectral changes of gallium corroles. With the gradual increase of CT-DNA concentration, the absorbance intensity of the Soret band of several gallium corroles gradually decreased. Although the hypochromism of these gallium corroles existed, no obvious red shift or blue shift was observed at the Soret band. It could be speculated that these gallium corroles bound to DNA via an outside binding mode.[24] In addition, the increase of CT-DNA to **1-Ga** solution led to a 28.62% hypochromicity and a bathochromic shift of 1 nm, and the intrinsic binding constant (K_b) between **1-Ga** and CT-DNA came out to be 1.04 × 10^5 M^{-1}, which was larger than other gallium corroles. This implied that compared to other gallium corroles, **1-Ga** may have stronger interaction with CT-DNA. All spectroscopic titration data are listed in Table 2.

The fluorescence spectrum titration experiment is also a common method to study the interaction between complexes and DNA. The fluorescence of complexes is usually enhanced when the complexes are inserted into DNA base pairs, as DNA prevents the complexes from colliding with solvent molecules.[25] However, the fluorescence spectrum can also change if the complexes interacted with DNA in other ways. Figure 3 shows the fluorescence spectrum of these gallium corroles interacted with CT-DNA. With the increase of CT-DNA concentration, the intensity of the fluorescence of these gallium corroles gradually weakened. It could be inferred that these gallium corroles had some interaction with CT-DNA. Also, **1-Ga** had a stronger interaction with CT-DNA according to the quenching constant (K_{sv}), which was consistent with the consequence of absorption spectrum titration experiment.

https://dx.doi.org/10.1021/acs.inorgchem.0c03016
Inorg. Chem. 2021, 60, 2234−2245

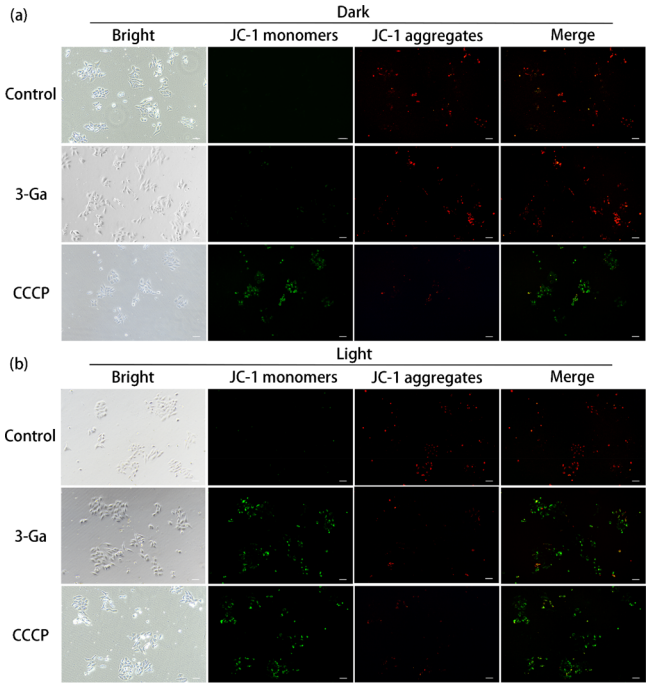

Figure 7. Mitochondrial membrane potential destruction of HepG2 cells induced by **3-Ga** (10 μM) under (a) dark or (b) light (625 ± 2 nm, 3 W/m^2, 1 h) by using JC-1 as fluorescence probe (scale bar is 100 μm); chloro carbonyl cyanide phenyl hydrazone (CCCP) is used as the positive control.

Photodynamic Properties. The ability of a photosensitizer to produce singlet oxygen is the key to evaluate the treatment effect in photodynamic therapy. The photosensitizers transfer from the ground state to the excited state upon irradiation, then cross back to the ground state through inter system crossing and transfer energy to triplet molecular oxygen to generate singlet oxygen, which is considered to play a major role in cell killing.[26] The single oxygen yield of prepared gallium corroles were measured indirectly by using DPBF, as shown in Figure 4a, after adding prepared gallium corroles into the DPBF solution, the absorbance of DPBF decreased with the illumination time, indicating that the synthesized gallium corroles produced singlet oxygen under the light condition. From Figure 4, although it seems that **4-Ga** has the highest $^1O_2$ production quantum yield, the calculated $^1O_2$ quantum yield of **4-Ga** is lower than that of **3-Ga** due to its significant higher molar extinction coefficient at illumination wavelength 625 nm (eq 3). Also, **3-Ga** has the strongest ability to produce singlet oxygen, whose singlet oxygen yield ($\Phi_\triangle$) is 0.32 (Table 1).

The photo-induced singlet oxygen was further investigated by EPR with TEMP serving as the trapping agent. Upon irradiation with a 625 nm laser for 1 min, a significant intensive EPR signal appeared (Figure 4b–e), which was in accordance with a typical EPR spectrum of the TEMPO-$^1O_2$ adducts with a three-line signal of 1:1:1.[27] After the addition of quenching agent, DABCO, the signal was dramatically weakened, which further proved the generation of singlet oxygen.

The self-aggregation of porphyrins in solution is very common, mainly due to strong attractive interactions between conjugation structures, but it will reduce the activity of porphyrins.[28] Therefore, we studied aggregation behavior of prepared gallium corroles by UV–vis spectra in DMF and DMF/Tris–HCl (pH 7.2) buffer mixture solution. Whether it was in DMF or DMF/Tris solutions, there was no significant red shift or blue shift in the Soret band (Figures S33–S34), indicating that gallium corroles did not aggregate within the range of concentration tested.

Photostability is an important index of PDT and photochemical reaction photosensitizers. The photostability of gallium corroles were examined by observing the bleaching of the Soret band under illumination. With the increase of exposure time, gallium corroles showed different degrees of bleaching (Figure S35), among which **2-Ga** was the most obvious, while **3-Ga** showed good photostability.

Cytotoxicity. The cytotoxicity of gallium corroles were detected by the MTT assay under dark or light conditions against three cancer cells, A549 (lung), 231 (breast), HepG2 (liver), and two normal cells, HSF and Huvec. Succinic acid dehydrogenase in the mitochondria of living cells reduced exogenous MTT into water-insoluble blue-purple crystal formazan.[29] After formazan deposited in the cells, DMSO was added to dissolve it and the cell viability could be indirectly reflected by the absorbance at 495 nm. The IC_{50} values of several gallium corroles to different cells are summarized in Table 3. The dark toxicity and phototoxicity of gallium corroles toward tumor cells depended on the type of cell, while these gallium corroles had little toxicity to two normal cells under dark conditions. At the same time, **1-Ga** had little dark toxicity but high phototoxicity against two tested normal cells. **4-Ga** also exhibited significant phototoxicity to normal cells HSF. In contrast, **3-Ga** showed low cytotoxicity to all tested normal cells under both light and dark conditions, but high phototoxicity to HepG2 liver cancer cells with an IC50 value of 10.0 ± 1.6 μM. It displayed a remarkable dark–light cytotoxicity difference in inducing HepG2 toxicity too. The phototoxicity of **3-Ga** toward HepG2 cells is even comparable to clinically used photosensitizer temoporfin. Also, of all prepared corrole photosensitizers, **3-Ga** showed minimal toxicity to tested normal cells whether under light or dark conditions. Encouraged by above results, we further explored photodynamic performance of **3-Ga** in HepG2 cells.

Cellular Uptake. Stimulated by the good phototoxicity of **3-Ga** toward HepG2 cells, we tested its uptake in HepG2 cells. Even though the mechanisms of uptake of gallium corroles remain unknown, chemical properties such as lower molecular weight (Mr), smaller polar surface area (tPSA), and higher lipophilicity (cLogP) have been proved to enhance cellular uptake of drugs.[30] Therefore, we first used ChemDraw software to obtain the related properties of several prepared gallium corroles (Table 4). Compared with the previously reported carboxylated gallium corroles,[30a] **3-Ga** showed lower Mr, smaller tPSA, and larger cLogP, which may enhance cell uptake and permeability. For cellular uptake experiment, cells were treated with **3-Ga** and stained with DAPI, which is a blue fluorescent dye that strongly binds to DNA. The uptake results of **3-Ga** by HepG2 cells were depicted in Figure 5. Obviously, the strong red fluorescence in HepG2 cells indicated the effective uptake of **3-Ga** by HepG2 cells. Also, the red fluorescence was distributed around the nucleus, mainly in the cytoplasm (Figure 5a). In addition, the flow cytometry was also used to investigate the time-dependent uptake of **3-Ga** in HepG2 (Figure 5b). The intracellular fluorescence intensity increased about one order at the first 2 h incubation. With the further extension of culture time from 2 to 6 h, the intracellular fluorescence intensity increased slightly. These observations

https://dx.doi.org/10.1021/acs.inorgchem.0c03016
Inorg. Chem. 2021, 60, 2234–2245

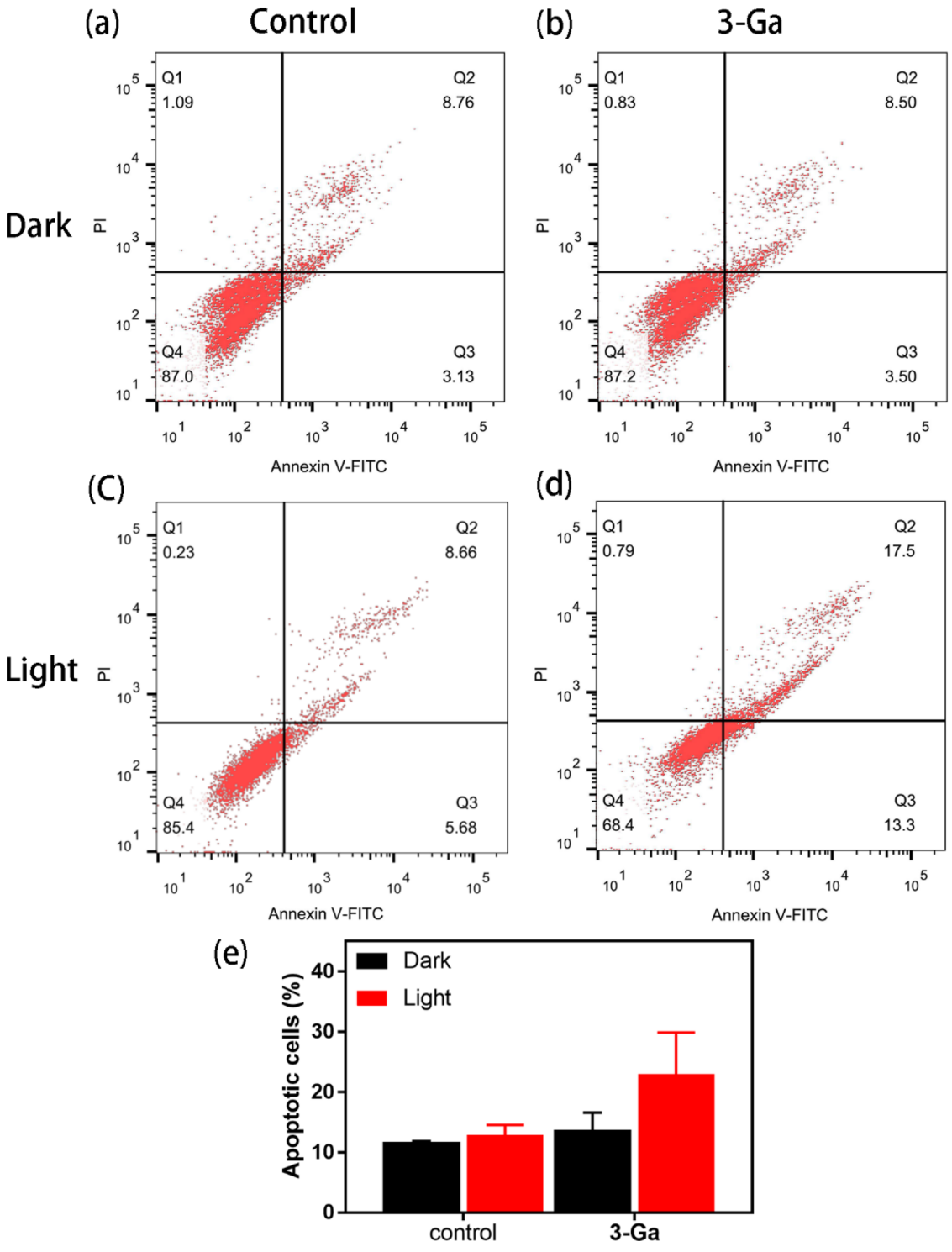

Figure 8. Annexin-V FITC and propidiun iodide (PI) staining of HepG2 cells by flow cytometry analysis. (a) Control group in the dark, (b) cells treated with **3-Ga** (10 μM) in the dark, (c) cells in the light, (d) cells treated with **3-Ga** (10 μM) and irradiation (625 $\pm$ 2 nm, 3 W/m^2, 1 h), and (e) data of late apoptotic (AV+/PI+) cells in the different groups.

indicated that **3-Ga** could efficiently penetrate HepG2 cells without the addition of any external carrier protein and was mainly localized in the cytoplasm. This is different from previously reported gallium sulfonated corrole in which the additive carrier protein is needed to assist the cellular uptake.[15a] Since the gallium corrole **3-Ga** could not enter the nucleus, its interaction with nuclei DNA was not possible and the mutagenic risk was avoided. This is the advantage of **3-Ga** as an ideal photosensitizer.

Detection of Intracellular ROS. The production of reactive oxygen species (ROS) plays an important role in the process of cell death and has been thought to regulate the process involved in the initiation of apoptotic signaling.[31] Herein, we used 2′,7′-dichlorodihydrofluorescein diacetate (DCFH-DA) and Rosup as fluorescent dyes and positive

https://dx.doi.org/10.1021/acs.inorgchem.0c03016
Inorg. Chem. 2021, 60, 2234−2245

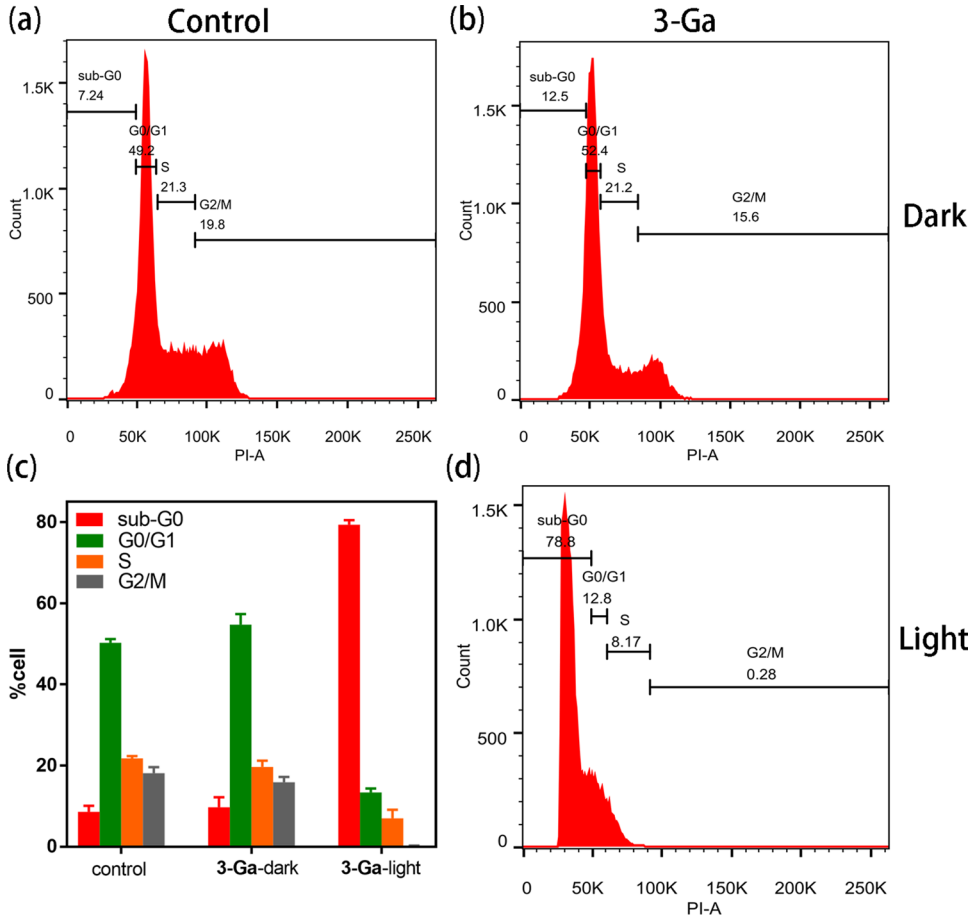

Figure 9. Cell cycle distribution of HepG2 by flow cytometry analysis. (a) Control group, (b) cells treated with **3-Ga** (10 μM) in the dark, and (d) cells treated with **3-Ga** (10 μM) and irradiation (625 ± 2 nm, 3 W/m^2, 1 h). (c) Graph of the cell cycle distribution.

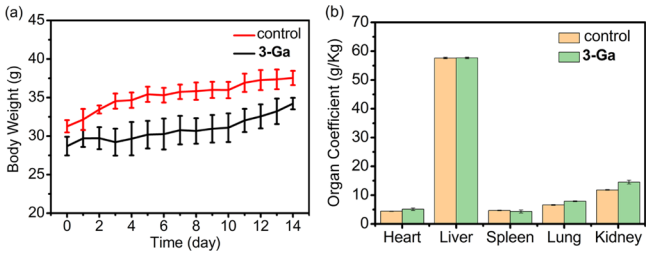

Figure 10. In vivo acute toxicity of gallium corrole **3-Ga**. (a) Body weight changes, (b) organ coefficients.

controls, respectively, to detect the ROS production of **3-Ga** in HepG2 cells. DCFH-DA itself has no fluorescence, but it can pass through the cell membrane freely and enter the cell. After entering the cell, it can be hydrolyzed by intracellular esterase to produce DCFH. Intracellular ROS can oxidize the non-fluorescent DCFH to produce the compound DCF with green fluorescence. The level of intracellular ROS can be determined by measuring the fluorescence of DCF. As shown in Figure 6, no green fluorescence was observed in cells treated with light and **3-Ga** alone, which has no difference when compared with the control group. However, in the **3-Ga** + light group, obvious green fluorescence could be observed, indicating that the ROS level in HepG2 cells was significantly increased, which was similar to the positive control group. These results suggested that **3-Ga** had little ability to produce ROS in the dark. Nevertheless, its ability to generate ROS is activated under laser irradiation, resulting in oxidative damage of cells, which is an important condition as a potential PDT photosensitizer for the treatment of liver cancer.

Mitochondrial Membrane Potential Assay. The loss of mitochondrial membrane potential is one of the key events of cell apoptosis and the decrease of mitochondrial membrane potential indicates the occurrence of early cell apoptosis.[32] JC-1 is a kind of fluorescent probe widely used to detect the mitochondrial membrane potential. When the mitochondrial membrane potential is high, JC-1 aggregates in the mitochondrial matrix to form a polymer that can emit red fluorescence; when the mitochondrial membrane potential is low, JC-1 exists as a monomer and emits green fluorescence. Hence, the decrease of the mitochondrial membrane potential can be easily detected by fluorescence color transformation of JC-1, which can also be regarded as an indicator of early apoptosis. As shown in Figure 7, much like the control group, JC-1 effectively aggregated and emitted red fluorescence in cells treated with light and **3-Ga** alone, attributed to a high mitochondrial membrane potential. However, the group of **3-Ga** + light was consistent with the positive control group, JC-1 existed in a monomer form and emitted green fluorescence, indicating that the mitochondrial membrane potential of HepG2 cells treated with **3-Ga** PDT was significantly decreased. These results further demonstrate that **3-Ga** has no obvious damage to cells in the dark, while under light conditions, **3-Ga** is highly toxic and may induce apoptosis of HepG2 cells.

https://dx.doi.org/10.1021/acs.inorgchem.0c03016
Inorg. Chem. 2021, 60, 2234−2245

Apoptosis Assay. For apoptosis assay, the cells were simultaneously stained with Annexin V-FITC and propidium iodide (PI). Annexin V-FITC staining can directly detect phosphatidylserine valgus, an important feature of apoptosis, and PI can stain necrotic cells or cells that have lost membrane integrity in late-stage apoptosis. The necrotic cells, late-stage apoptotic cells, early-stage apoptotic cells, and living cells correspond to quadrants 1, 2, 3, and 4, respectively. As is shown in Figure 8c, cell apoptosis percentage treated with **3-Ga** under dark conditions showed little difference to the control group (13.65% and 11.67%, respectively), while the apoptosis ratio of cells treated with **3-Ga** under illumination was twice more than that of the control group. Meanwhile, the HepG2 cell viability after PDT treatment with **3-Ga** dropped to 68.4% and the percentage of apoptotic and necrotic cells reached 30.8% (Figure 8d). These results suggested that **3-Ga** could lead to apoptosis under light conditions while having less dark toxicity, which was consistent with previous experimental results.

Cell Cycle Assay. In order to investigate the potential mechanism of prepared gallium corrole induced cytotoxic effect, we used flow cytometry to detect the cell cycle distribution. HepG2 cells after PDT treatment with samples showed significant changes in cell cycle. As depicted in Figure 9, compared with the control group, HepG2 cell cycle distribution treated with **3-Ga** under dark condition did not exhibit significant changes, indicating that **3-Ga** had little influence on cell cycle distribution under dark conditions. While under the light conditions, after **3-Ga** treatment, the percentage of cells during sub-G0 phase increased from 7.24 to 78.8%, and the percentage of cells in other phases all decreased sharply, which is mainly due to cell apoptosis caused by **3-Ga**.

In Vivo Acute Toxicity. It is necessary to carry out toxicological experiments for the safe application of drugs in biomedicine. Therefore, healthy BALB/c mice were chosen for a simple assessment of acute toxicity of **3-Ga** in vivo. As shown in Figure 10a, the body weight of mice in the experimental groups and control groups increased steadily within 2 weeks after administration, and no abnormalities or lesions were observed in all mice during the observation period, indicating that **3-Ga** basically did not affect the normal growth of mice. In addition, Figure 10b shows that organ coefficients of mice treated with **3-Ga** were not significantly different from those of the control groups, and there were no significant changes in the appearance of major organs (Figure S36). Based on the above results, **3-Ga** may have no obvious acute toxicity in BALB/C mice when the tail vein injection dose is no more than 10 mg/kg. More detailed and in-depth biochemical analysis is needed to demonstrate that 10 mg/kg of **3-Ga** is a safe dose for BALB/c mice.

CONCLUSION

In summary, we prepared a series of new halogenated gallium corroles for photodynamic therapy. These gallium corroles bind to CT-DNA via an outside binding mode and can efficiently produce singlet oxygen under light illumination. Among all synthesized gallium corroles, **3-Ga** has the best photodynamic antitumor activity against HepG2 cells. The fluorescence microscope showed that **3-Ga** could entrance HepG2 cells smoothly, generate ROS in cells after illumination, and lead to the destruction of the cell mitochondrial membrane potential. Flow cytometry results further showed that **3-Ga** could lead to an increase of cells at the sub-G0 phase after illumination, which corresponds to cell apoptosis. In addition, the in vivo test showed that **3-Ga** had very low acute toxicity at a dose of 10 mg/kg. The preliminary results showed that **3-Ga** is a promising PDT photosensitizer.

ASSOCIATED CONTENT

Supporting Information

The Supporting Information is available free of charge at https://pubs.acs.org/doi/10.1021/acs.inorgchem.0c03016.

Details of characterization data, including NMR, HRMS, and FT-IR spectral data, aggregation, photo-degradation, and acute toxicity study (PDF)

AUTHOR INFORMATION

Corresponding Authors

Yu-Hui Liao − *Molecular Diagnosis and Treatment Center for Infectious Diseases, Dermatology Hospital, Southern Medical University, Guangzhou 510091, China;* orcid.org/0000-0003-4702-9516; Email: liaoyh8@mail.sysu.edu.cn

Hai-Yang Liu − *School of Chemistry and Chemical Engineering, Key Laboratory of Functional Molecular Engineering of Guangdong Province, South China University of Technology, Guangzhou 510641, China;* orcid.org/0000-0002-1793-952X; Email: chhyliu@scut.edu.cn

Authors

Ling-Gui Liu − *School of Chemistry and Chemical Engineering, Key Laboratory of Functional Molecular Engineering of Guangdong Province, South China University of Technology, Guangzhou 510641, China*

Yan-Mei Sun − *School of Chemistry and Chemical Engineering, Key Laboratory of Functional Molecular Engineering of Guangdong Province, South China University of Technology, Guangzhou 510641, China*

Ze-Yu Liu − *School of Chemistry and Chemical Engineering, Key Laboratory of Functional Molecular Engineering of Guangdong Province, South China University of Technology, Guangzhou 510641, China*

Lei Zeng − *Foresea Life Insurance Guangzhou General Hospital, Guangzhou 511300, China*

Yong Ye − *School of Chemistry and Chemical Engineering, Key Laboratory of Functional Molecular Engineering of Guangdong Province, South China University of Technology, Guangzhou 510641, China;* orcid.org/0000-0002-9535-8800

Complete contact information is available at: https://pubs.acs.org/10.1021/acs.inorgchem.0c03016

Funding

We gratefully acknowledge financial support from the National Natural Science Foundation of China (no. 21671068).

Notes

The authors declare no competing financial interest.

REFERENCES

(1) (a) Zhou, X.; Li, H.; Shi, C.; Xu, F.; Zhang, Z.; Yao, Q.; Ma, H.; Sun, W.; Shao, K.; Du, J.; Long, S.; Fan, J.; Wang, J.; Peng, X. An APN-activated NIR photosensitizer for cancer photodynamic therapy and fluorescence imaging. *Biomaterials* **2020**, *253*, 120089. (b) Yu, Z.; Xia, Y.; Xing, J.; Li, Z.; Zhen, J.; Jin, Y.; Tian, Y.; Liu, C.; Jiang, Z.; Li, J.; Wu, A. Y_1-receptor-ligand-functionalized ultrasmall upconversion nanoparticles for tumor-targeted trimodality imaging and photo-

dynamic therapy with low toxicity. *Nanoscale* **2018**, *10*, 17038−17052.
(2) Teo, R. D.; Hwang, J. Y.; Termini, J.; Gross, Z.; Gray, H. B. Fighting Cancer with Corroles. *Chem. Rev.* **2017**, *117*, 2711−2729.
(3) (a) Spikes, J. D. New trends in photobiology: Chlorins as photosensitizers in biology and medicine. *J. Photochem. Photobiol., B* **1990**, *6*, 259−274. (b) Berg, K.; Selbo, P. K.; Weyergang, A.; Dietze, A.; Prasmickaite, L.; Bonsted, A.; Engesaeter, B. Ø.; Angell-Petersen, E.; Warloe, T.; Frandsen, N.; Høgset, A. Porphyrin-related photosensitizers for cancer imaging and therapeutic applications. *J. Microsc.* **2005**, *218*, 133−147. (c) Stylli, S. S.; Howes, M.; MacGregor, L.; Rajendra, P.; Kaye, A. H. Photodynamic therapy of brain tumours: evaluation of porphyrin uptake versus clinical outcome. *J. Clin. Neurosci.* **2004**, *11*, 584−596.
(4) (a) Nardis, S.; Mandoj, F.; Stefanelli, M.; Paolesse, R. Metal complexes of corrole. *Coord. Chem. Rev.* **2019**, *388*, 360−405. (b) Gross, Z.; Galili, N.; Saltsman, I. The first direct synthesis of corroles from pyrrole. *Angew. Chem., Int. Ed.* **1999**, *38*, 1427−1429.
(5) Sharma, V. K.; Mahammed, A.; Soll, M.; Tumanskii, B.; Gross, Z. Corroles and corrole/transferrin nanoconjugates as candidates for sonodynamic therapy. *Chem. Commun.* **2019**, *55*, 12789−12792.
(6) Santos, C. I. M. Corroles: Synthesis, Functionalization and Application as Chemosensors. *ChemistryOpen* **2014**, *3*, 88−92.
(7) Sudhakar, K.; Mahammed, A.; Chen, Q.-C.; Fridman, N.; Tumanskii, B.; Gross, Z. Copper Complexes of CF3-Substituted Corroles for Affecting Redox Potentials and Electrocatalysis. *ACS Appl. Energy Mater.* **2020**, *3*, 2828−2836.
(8) (a) Dasari, S.; Tchounwou, P. B. Cisplatin in cancer therapy: Molecular mechanisms of action. *Eur. J. Pharmacol.* **2014**, *740*, 364−378. (b) Palchaudhuri, R.; Hergenrother, P. J. DNA as a target for anticancer compounds: methods to determine the mode of binding and the mechanism of action. *Curr. Opin. Biotechnol.* **2007**, *18*, 497−503.
(9) (a) Huang, J.-T.; Wang, X.-L.; Zhang, Y.; Mahmood, M. H. R.; Huang, Y.-Y.; Ying, X.; Ji, L.-N.; Liu, H.-Y. DNA binding and nuclease activity of a water-soluble sulfonated manganese(III) corrole. *Transition Met. Chem.* **2013**, *38*, 283−289. (b) Xie, A.-N.; Zhang, Z.; Wang, H.-H.; Ali, A.; Zhang, D.-X.; Wang, H.; Ji, L.-N.; Liu, H.-Y. DNA-binding, photocleavage and anti-cancer activity of tin(IV) corrole. *J. Porphyrins Phthalocyanines* **2018**, *22*, 739−750. (c) Zhang, Z.; Wen, J.-Y.; Lv, B.-B.; Li, X.; Ying, X.; Wang, Y.-J.; Zhang, H.-T.; Wang, H.; Liu, H.-Y.; Chang, C. K. Photocytotoxicity and G-quadruplex DNA interaction of water-soluble gallium(III) tris(N-methyl-4-pyridyl)corrole complex. *Appl. Organomet. Chem.* **2016**, *30*, 132−139.
(10) (a) Gorman, A.; Killoran, J.; O'Shea, C.; Kenna, T.; Gallagher, W. M.; O'Shea, D. F. In vitro demonstration of the heavy-atom effect for photodynamic therapy. *J. Am. Chem. Soc.* **2004**, *126*, 10619−10631. (b) Azenha, E. G.; Serra, A. C.; Pineiro, M.; Pereira, M. M.; de Melo, J. S.; Arnaut, L. G.; Formosinho, S. J.; Gonsalves, A. R. Heavy-atom effects on metalloporphyrins and polyhalogenated porphyrins. *Chem. Phys.* **2002**, *280*, 177−190. (c) Zhao, F.; Zhan, X.; Lai, S.-H.; Zhang, L.; Liu, H.-Y. Photophysical properties and singlet oxygen generation of meso-iodinated free-base corroles. *RSC Adv.* **2019**, *9*, 12626−12634. (d) Liu, H.-Y.; Guo, P.-Y.; Kong, P.-W.; Ying, X.; Liao, S.-J.; Mak, N.-K.; Chang, C.-K. Heavy-atom effect of corrole photosensitizer for photodynamic therapy. *Chem. J. Chin. Univ.* **2006**, *27*, 1363−1365.
(11) (a) You, L.; Shen, H.; Shi, L.; Zhang, G.; Liu, H.; Wang, H.; Ji, L. Photophysical properties of the Corrole photosensitizers. *Sci. China: Phys., Mech. Astron.* **2010**, *53*, 1491−1496. (b) Shi, L.; Liu, H.-Y.; Shen, H.; Hu, J.; Zhang, G.-L.; Wang, H.; Ji, L.-N.; Chang, C.-K.; Jiang, H.-F. Fluorescence properties of halogenated mono-hydroxyl corroles: the heavy-atom effects. *J. Porphyrins Phthalocyanines* **2009**, *13*, 1221−1226.
(12) (a) Mahammed, A.; Gross, Z. Corroles as triplet photosensitizers. *Coord. Chem. Rev.* **2019**, *379*, 121−132. (b) Shao, W.; Wang, H.; He, S.; Shi, L.; Peng, K.; Lin, Y.; Zhang, L.; Ji, L.; Liu, H. Photophysical Properties and Singlet Oxygen Generation of Three Sets of Halogenated Corroles. *J. Phys. Chem. B* **2012**, *116*, 14228−14234. (c) Shi, L.; Liu, H. Y.; Si, L. P.; Peng, K. M.; You, L. L.; Wang, H.; Zhang, L.; Ji, L. N.; Chang, C. K.; Jiang, H. F. The heavy atom effect on photocleavage of DNA by mono-hydroxyl halogenated corroles. *Chin. Chem. Lett.* **2010**, *21*, 373−375.
(13) Soll, M.; Goswami, T. K.; Chen, Q.-C.; Saltsman, I.; Teo, R. D.; Shahgholi, M.; Lim, P.; Di Bilio, A. J.; Cohen, S.; Termini, J.; Gray, H. B.; Gross, Z. Cell-Penetrating Protein/Corrole Nanoparticles. *Sci. Rep.* **2019**, *9*, 2294.
(14) (a) Zhang, Z.; Wang, H.-H.; Yu, H.-J.; Xiong, Y.-Z.; Zhang, H.-T.; Ji, L.-N.; Liu, H.-Y. Synthesis, characterization and in vitro and in vivo photodynamic activities of a gallium(III) tris(ethoxycarbonyl)-corrole. *Dalton Trans.* **2017**, *46*, 9481−9490. (b) Cheng, F.; Huang, L.; Wang, H.; Liu, Y.; Kandhadi, J.; Wang, H.; Ji, L.; Liu, H. Photodynamic Therapy Activities of 10-(4-Formylphenyl)-5,15-bis-(pentafluorophenyl)corrole and Its Gallium Complex. *Chin. J. Chem.* **2017**, *35*, 86−92. (c) Chen, X.; Wang, H.-H.; Akram, W.; Sun, Y.-M.; Liao, Y.-H.; Si, L.-P.; Liu, H.-Y.; Chang, C.-K. Tri-hydroxyl Corrole and Its Gallium(III) Complex: DNA-Binding, Photocleavage and in Vitro Photodynamic Antitumor Activities. *Chin. J. Inorg. Chem.* **2019**, *35*, 1687−1697.
(15) (a) Agadjanian, H.; Weaver, J. J.; Mahammed, A.; Rentsendorj, A.; Bass, S.; Kim, J.; Dmochowski, I. J.; Margalit, R.; Gray, H. B.; Gross, Z.; Medina-Kauwe, L. K. Specific delivery of corroles to cells via noncovalent conjugates with viral proteins. *Pharm. Res.* **2006**, *23*, 367−377. (b) Agadjanian, H.; Ma, J.; Rentsendorj, A.; Valluripalli, V.; Hwang, J. Y.; Mahammed, A.; Farkas, D. L.; Gray, H. B.; Gross, Z.; Medina-Kauwe, L. K. Tumor detection and elimination by a targeted gallium corrole. *Proc. Natl. Acad. Sci. U. S. A.* **2009**, *106*, 6105−6110.
(16) (a) Sun, Y.-M.; Akram, W.; Cheng, F.; Liu, Z.-Y.; Liao, Y.-H.; Ye, Y.; Liu, H.-Y. DNA interaction and photodynamic antitumor activity of transition metal mono-hydroxyl corrole. *Bioorg. Chem.* **2019**, *90*, 103085. (b) Sun, Y.-M.; Jiang, X.; Liu, Z.-Y.; Liu, L.-G.; Liao, Y.-H.; Zeng, L.; Ye, Y.; Liu, H.-Y. Hydroxy-corrole and its gallium(III) complex as new photosensitizer for photodynamic therapy against breast carcinoma. *Eur. J. Med. Chem.* **2020**, *208*, 112794−112794.
(17) Tjahjono, D. H.; Yamamoto, T.; Ichimoto, S.; Yoshioka, N.; Inoue, H. Synthesis and DNA-binding properties of bisdiazoliumyl-porphyrins. *J. Chem. Soc., Perkin Trans. 1* **2000**, 3077−3081.
(18) Lakowicz, J. R.; Weber, G. Quenching of protein fluorescence by oxygen. Detection of structural fluctuations in proteins on the nanosecond time scale. *Biochemistry* **1973**, *12*, 4171−4179.
(19) Thomas, A. P.; Saneesh Babu, P. S.; Asha Nair, S.; Ramakrishnan, S.; Ramaiah, D.; Chandrashekar, T. K.; Srinivasan, A.; Radhakrishna Pillai, M. Meso-Tetrakis(p-sulfonatophenyl)N-Confused Porphyrin Tetrasodium Salt: A Potential Sensitizer for Photodynamic Therapy. *J. Med. Chem.* **2012**, *55*, 5110−5120.
(20) Giribabu, L.; Jain, K.; Sudhakar, K.; Duvva, N.; Chitta, R. Light induced intramolecular electron and energy transfer events in rigidly linked borondipyrromethene: Corrole Dyad. *J. Lumin.* **2016**, *177*, 209−218.
(21) Seybold, P. G.; Gouterman, M. Porphyrins. XIII. Fluorescence spectra and quantum yields. *J. Mol. Spectrosc.* **1969**, *31*, 1−13.
(22) Redmond, R. W.; Gamlin, J. N. A compilation of singlet oxygen yields from biologically relevant molecules. *Photochem. Photobiol.* **1999**, *70*, 391−475.
(23) Pasternack, R. F.; Gibbs, E. J.; Villafranca, J. J. Interactions of porphyrins with nucleic acids. *Biochemistry* **1983**, *22*, 2406−2414.
(24) Da Silveira, C. H.; Garoforo, E. N.; Chaves, O. A.; Gonçalves, P. F. B.; Streit, L.; Iglesias, B. A. Synthesis, spectroscopy, electrochemistry and DNA interactive studies of meso-tetra(1-naphthyl)porphyrin and its metal complexes. *Inorg. Chim. Acta* **2018**, *482*, 542−553.
(25) Maheswari, P. U.; Palaniandavar, M. DNA binding and cleavage activity of Ru(NH3)(4)(diimine) Cl-2 complexes. *Inorg. Chim. Acta* **2004**, *357*, 901−912.

https://dx.doi.org/10.1021/acs.inorgchem.0c03016
Inorg. Chem. 2021, 60, 2234−2245

(26) Ethirajan, M.; Chen, Y.; Joshi, P.; Pandey, R. K. The role of porphyrin chemistry in tumor imaging and photodynamic therapy. *Chem. Soc. Rev.* **2011**, *40*, 340−362.
(27) Fu, H.-G.; Chen, Y.; Yu, Q.; Liu, Y. A tumor-targeting Ru/polysaccharide/protein supramolecular assembly with high photodynamic therapy ability. *Chem. Commun.* **2019**, *55*, 3148−3151.
(28) (a) Da Silveira, C. H.; Vieceli, V.; Clerici, D. J.; Santos, R. C. V.; Iglesias, B. A. Investigation of isomeric tetra-cationic porphyrin activity with peripheral Pd(bpy)Cl + units by antimicrobial photodynamic therapy. *Photodiagn. Photodyn. Ther.* **2020**, *31*, 101920. (b) Oliveira, V. A.; Terenzi, H.; Menezes, L. B.; Chaves, O. A.; Iglesias, B. A. Evaluation of DNA-binding and DNA-photocleavage ability of tetra-cationic porphyrins containing peripheral Ru(bpy)2Cl + complexes: Insights for photodynamic therapy agents. *J. Photochem. Photobiol., B* **2020**, *211*, 111991.
(29) Mosmann, T. Rapid colorimetric assay for cellular growth and survival: application to proliferation and cytotoxicity assays. *J. Immunol. Methods* **1983**, *65*, 55−63.
(30) (a) Pribisko, M.; Palmer, J.; Grubbs, R. H.; Gray, H. B.; Termini, J.; Lim, P. Cellular uptake and anticancer activity of carboxylated gallium corroles. *Proc. Natl. Acad. Sci. U. S. A.* **2016**, *113*, E2258−E2266. (b) Giordanetto, F.; Kihlberg, J. Macrocyclic Drugs and Clinical Candidates: What Can Medicinal Chemists Learn from Their Properties? *J. Med. Chem.* **2014**, *57*, 278−295.
(31) Wang, Y.; He, Q. Y.; Sun, R. W. Y.; Che, C. M.; Chiu, J. F. Gold(III) porphyrin 1a induced apoptosis by mitochondrial death pathways related to reactive oxygen species. *Cancer Res.* **2005**, *65*, 11553−11564.
(32) Green, D. R.; Reed, J. C. Mitochondria and apoptosis. *Science* **1998**, *281*, 1309−1312.

https://dx.doi.org/10.1021/acs.inorgchem.0c03016
Inorg. Chem. 2021, 60, 2234−2245